Electronic Supporting Information for: Simulation of experimental imaging results for the OH+CHD_3 reaction with a simple and accurate theoretical approach

Laurent Bonnet[1,2] and Joaquin Espinosa-Garcia[3]
[1] *CNRS, Institut des Sciences Moléculaires, UMR 5255, 33405, Talence, France*
[2] *Univ. Bordeaux, Institut des Sciences Moléculaires, UMR 5255, 33405, Talence, France*
[3] *Departamento de Química Física, Universidad de Extremadura, Avenida de Elvas S/N, 06071 Badajoz, Spain*

I. QCT-1GB CALCULATIONS

We used the VENUS code [1] to run 10^6 trajectories on the PES-2014 for each process. Full computational details on these calculations can be found in refs. [2, 3]. 85587 and 75277 trajectories were found to be reactive for channels (i) H_2O+CD_3 and (ii) HOD+CHD_2, respectively.

A. H_2O+CD_3 channel

1. Product outcomes

The product dynamical quantities involved in the next developments are the vibrational energy $E^{vib}_{CD_3}$ of CD_3, its rotational energy $E^{rot}_{CD_3}$, the vibrational energy $E^{vib}_{H_2O}$ of co-fragment H_2O, its rotational energy $E^{rot}_{H_2O}$, the vibrational actions a_1, a_2 and a_3 associated with the antisymmetric streching, symmetric streching and bending vibrational modes of H_2O, respectively, the relative translational energy E_{trans} between H_2O and CD_3, and the speed v of CD_3 within the center-of-mass system. The VENUS code provides directly all these quantities except the actions and the velocity. The actions are obtained from nuclear positions and velocities by means of the normal-mode analysis (NMA) method [4], which includes anharmonicity and Coriolis-coupling terms. v is deduced from E_{trans} by the relation [5]

$$v = \left[\frac{2E_{trans}}{m_{CD_3}\left(1 + \frac{m_{CD_3}}{m_{H_2O}}\right)} \right]^{1/2} . \quad (1)$$

This velocity is the one measured by Zhang *et al.* using the VMI technics [6].

2. Vibrational state populations

The vibrational quantum numbers (n_1,n_2,n_3) of H_2O are the quantum counterparts of the actions (a_1, a_2, a_3). The frequencies associated with these quantities are denoted ω_1, ω_2 and ω_3 (their values are given in ref. [3]). The population of state (n_1,n_2,n_3) is denoted $p_{n_1n_2n_3}$. In the experiments of Zhang *et al.* [6], frozen reagents meet with a collision energy of 10.7 kcal/mol and $P(v)$ is measured for CD_3 in its vibrational ground state and its lowest rotational levels ($N \leq 5$) [7]. The rotational energy $E^{rot}_{CD_3}$ of the probed CD_3 radical is thus lower than $\sim$ 1 kcal/mol. Four vibrational states are found to be available to H_2O. These states are (0,1,0), (1,0,0), (0,1,1) and (1,0,1), by increasing order of energy. The constraints imposed by the VMI technics are taken into account as follows: (i) the zero point energy (ZPE) of CD_3 is $E^0_{CD_3} = 13.85$ kcal/mol. We assume that all the trajectories violating the ZPE, i.e., such that $E^{vib}_{CD_3} < 13.85$, do not contribute to the reactivity. We thus discard them from the statistics; (ii) the energy of the first excited vibrational state of CD_3 is 14.98 kcal/mol, corresponding to one quantum in the lowest umbrella mode of CD_3 (1.13 kcal/mol) above the ZPE. We now assume, in the spirit of standard binning (SB) [8], that all the trajectories leading to $E^{vib}_{CD_3} > 14.98$ kcal/mol do not contribute to the vibrational ground state of CD_3 probed

by Zhang *et al.* [6], and should thus be ignored. We have thus doubled the width of the interval considered in our previous study (see condition (ii) in Section 2.2 of ref. [5]). In doing so, we significantly improve the statistics. (iii) finally, we also reject all the trajectories leading to $E^{rot}_{CD_3} > 1$ kcal/mol.

The 1GB estimation of the population $p_{n_1n_2n_3}$ of state (n_1, n_2, n_3) is performed as follows [3, 8–12]: we consider the set of trajectories for which $\bar{a}_1 = n_1$, $\bar{a}_2 = n_2$ and $\bar{a}_3 = n_3$, where $\bar{a}_i$ is the nearest integer of a_i, i =1, 2 or 3. In other words, trajectories for which (a_1, a_2, a_3) does not belong to the unit cube centred at (n_1,n_2,n_3) are rejected. Those belonging to the unit cube are assigned, within the realistic harmonic treatment of H_2O vibrations, the 1GB weight

$$p^{1GB}_{n_1n_2n_3}(a_1, a_2, a_3) = exp\left(-\frac{\rho^2}{\epsilon^2}\right) \tag{2}$$

with

$$\rho = \frac{\sum_{i=1}^{3} \omega_i(a_i - n_i)}{\sum_{i=1}^{3} \omega_i} \tag{3}$$

[3, 8–12]. The numerator in the right-hand-side (RHS) of the above equation is equal to the difference between the harmonic classical and quantum vibrational energies. Hence, the basic difference between the SB and 1GB procedures is that the latter puts strong emphasis on those trajectories leading to H_2O with its classical vibrational energy close to the energy of quantum state (n_1, n_2, n_3). When anharmonicities are not negligible, as will be the case for channel (ii) (see further below), this difference is replaced by the one between the exact classical and quantum vibrational energies [11, 12]. $p_{n_1n_2n_3}$ is obtained by summing the 1GB weights over the previous paths and normalizing to unity the whole set of populations. The resulting probabilities are represented in Fig. S1 in terms of ϵ. In principle, strictly applying Bohr quantization would require taking ϵ as close to 0 as possible [8, 10], so trajectories contributing to $p_{n_1n_2n_3}$ would be those leading to classical vibrational energies nearly equal to the energy of state (n_1,n_2,n_3). In practice, however, it is necessary to impose a lower bound to ϵ, as below this limit, the number of trajectories effectively contributing to the populations may not be statistically relevant. One may roughly identify this number as the amount of trajectories for which $p^{1GB}_{n_1n_2n_3}(a_1, a_2, a_3)$ is larger than 0.5 (see Eq. (2)). We call them 1GB paths from now on. Clearly, the number of 1GB paths decreases when ϵ decreases, due to the narrowing of the Gaussian width. The vertical red dashed line corresponds to $\epsilon = 0.028$, value leading to 100 1GB trajectories, which can be roughly considered as the minimum ensemble for a statistically meaningful estimation of the 1GB populations (by statistically meaningful estimation, we mean a prediction close to the one obtained from an infinite number of trajectories). On the right side of this line, we note that the populations vary almost linearly with ϵ. On the left side, the smaller ϵ, the smaller the statistics and the more irregular the variations of the populations. Since the experimental populations are assumed to be best described by the 1GB populations corresponding to $\epsilon = 0$, and the only statistically relevant 1GB populations are for $\epsilon \geq 0.028$, we deduce the former by linearly extrapolating the latter from $\epsilon = 0.028$ down to 0. Approximating the ϵ dependence of 1GB populations by straight lines passing through the points of the curves corresponding to $\epsilon = 0.028$ and 0.1 (see Fig. S1), we arrive at p^{1GB}_{010}, p^{1GB}_{100}, p^{1GB}_{011} and p^{1GB}_{101}. The 1GB populations given in the first two columns of Table I (rounded to their nearest integer) are deduced from the previous populations ($p^{1GB}_{01^{\pm}0} = p^{1GB}_{010} + p^{1GB}_{100}$, $p^{1GB}_{01^{\pm}1} = p^{1GB}_{011} + p^{1GB}_{101}$).

3. Pair-correlated speed distribution

The PCSD reads

$$P(v) = p_{010}P_{010}(v) + p_{100}P_{100}(v) + p_{011}P_{011}(v) + p_{101}P_{101}(v), \tag{4}$$

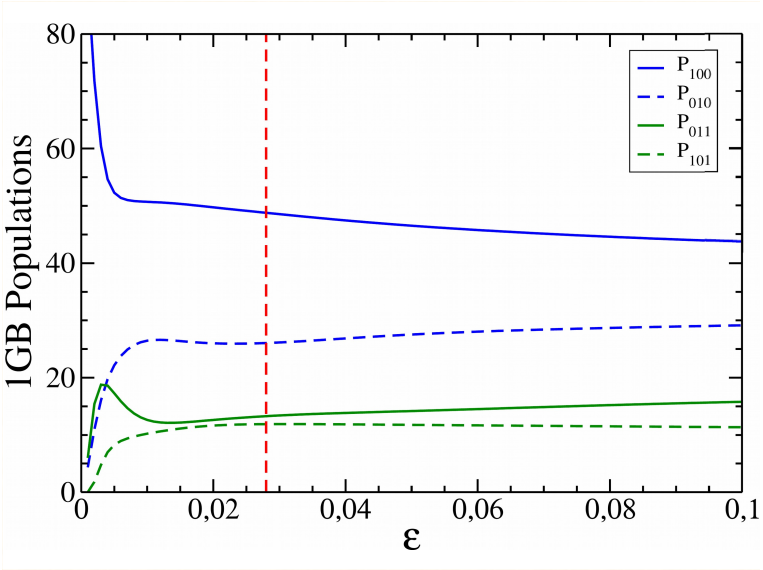

Fig. S 1: 1GB vibrational state populations (in percentage) of H_2O in terms of ϵ. The vertical red dashed line corresponds to the value of ϵ (0.028) such that 100 trajectories effectively contribute to the populations.

where $P_{n_1n_2n_3}(v)$ is the contribution of state (n_1,n_2,n_3) to $P(v)$ (the upperscript 1GB is not written anymore so as to avoid heavy notations). $P_{n_1n_2n_3}(v)$ is normalized to unity. In order to calculate it, we again focus on trajectories complying with VMI constraints and such that (a_1, a_2, a_3) belongs to the unit cube centred at (n_1,n_2,n_3). We then divide in 80 equal intervals the range [0.5, 2.5] comprising the velocities measured in km/s [6]. We identify the value of $P_{n_1n_2n_3}(v)$ at the center of a given interval with the sum of the 1GB weights of the trajectories leading to this interval, keeping ϵ at 0.028 in Eq. (2). The resulting curve is made of points separated by 0.025 km/s, thus leading to a satisfying resolution. Moreover, we repeat this calculation with $\epsilon = 0.014$ (not shown) and observe that despite more irregularities in $P_{n_1n_2n_3}(v)$ due to worse statistics, its width is nearly unchanged. The distribution at $\epsilon = 0.028$ is thus expected to be close to its extrapolation at $\epsilon = 0$. $P(v)$ as given by Eq. (4), however, should not be directly compared with the experimental PCSD for the following reason. In a hypothetical experiment where both reagents would be in the rovibrational ground state and the collision energy would be perfectly controlled, the total energy available to the products would take the same value for the whole set of reactions detected. Since E_{trans} is equal to the previous energy minus the quantized internal energy of the products, E_{trans} would also be quantized. Consequently, $P(v)$ would be given by a set of Dirac peaks with given weights. In our calculations, however, we pseudo-quantize the vibration motion through the 1GB procedure, but not the rotation motion. $P(v)$ is thus a rough approximation of what would be observed if the measurement of the final velocities would introduce a blurring of the peaks slightly exceeding the average spacing between them. In real experiments, however, the blurring is much larger, for the collision energy and the reagent rotational states are not fully controlled and VMI itself significantly contributes to the blurring. We thus take this into account in the calculation of the PCSD through the Gaussian convolution

$$P_c(v) = \int dv' \, \frac{1}{\sqrt{\pi}\eta} exp\left[-\left(\frac{v'-v}{\eta}\right)^2\right] P(v'). \tag{5}$$

The value of η is chosen so as to reproduce as satisfyingly as possible the experimental speed distribution at the threshold and cut-off. With η kept at 0.1, one obtains the 1GB curves in Figs. 1 and 3 (left panels).

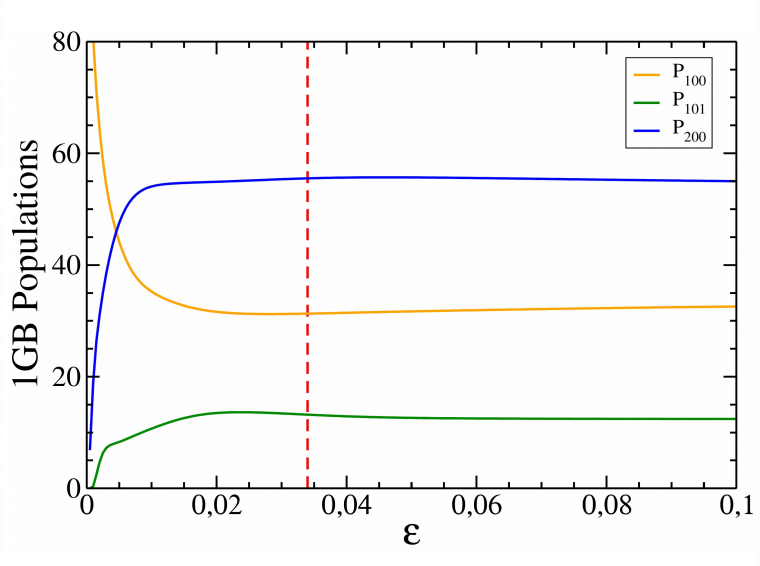

Fig. S 2: 1GB vibrational state populations (in percentage) of HOD in terms of ϵ. The vertical red dashed line corresponds to the value of ϵ (0.034) such that 100 trajectories effectively contribute to the populations.

B. HOD+CHD_2 channel

For this channel, the developments are similar as previously, with *ad-hoc* parameters in the mathematical expressions. However, they slightly differ in two respects. On one hand, regarding the VMI constraints on the vibrational energy of CHD_2, we apply condition (ii) in Section 2.2 of ref. [5]. Contrary to what we have done for channel (i), it is not necessary here to double the width of the interval considered in ref. [5] to improve the statistics. On the other hand, the difference $\sum_{i=1}^{3} \omega_i(a_i - n_i)$ between harmonic classical and quantum vibrational energies is replaced in Eq. (3) by the difference between exact classical and quantum vibrational energies in order to deal with anharmonicities [11, 12], larger for channel (ii) than for channel (i). More details on this substitution can be found in ref. [5]. Note that the set of trajectories used in the anharmonic case is still the one for which (a_1, a_2, a_3) belongs to the unit cube centred at (n_1,n_2,n_3). The ϵ-dependence of 1GB probabilities is represented in Fig. S2. The 1GB VSDs given in Table I and the 1GB PCSD displayed in Figs. 2 (left panel) and 3 (right panel) are calculated as previously explained.

II. QCT-GB CALCULATIONS

The calculations closely follow the previous ones. However, trajectories for which (a_1, a_2, a_3) belongs to the unit cube centred at (n_1,n_2,n_3) are not assigned the 1GB weights given by Eq. (2). Instead, they are assigned the Gaussian product

$$p^{GB}_{n_1 n_2 n_3}(a_1, a_2, a_3) = G_{n_1}(a_1) G_{n_2}(a_2) G_{n_3}(a_3) \tag{6}$$

with

$$G_n(a) = \frac{1}{\pi^{1/2}\epsilon} exp\left[-\left(\frac{a-n}{\epsilon} \right)^2 \right]. \tag{7}$$

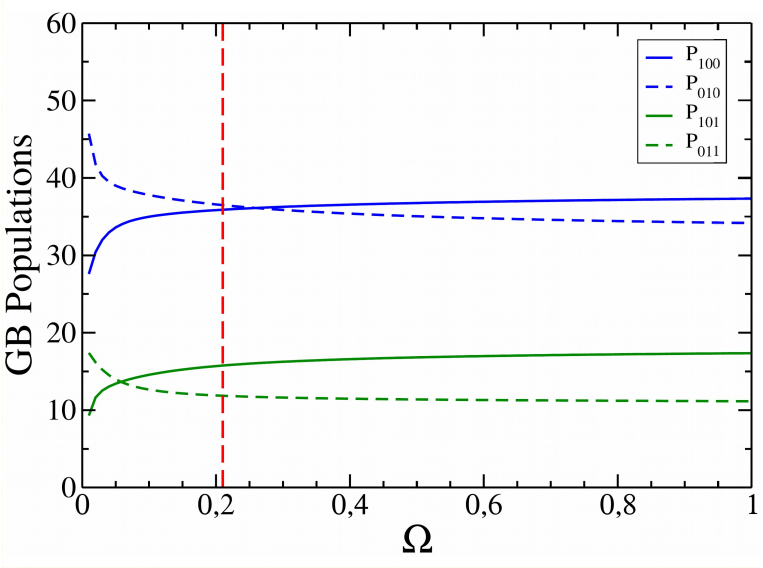

Fig. S 3: GB vibrational state populations (in percentage) of H_2O in terms of Ω. The vertical red dashed line corresponds to the value of Ω (0.21) such that 100 trajectories effectively contribute to the populations.

ϵ satisfies

$$\epsilon = \frac{\Omega^{\frac{1}{3}}}{2\,(ln2)^{1/2}}, \tag{8}$$

where Ω is the volume of the cube centered at (n_1,n_2,n_3), shown in the paper to mainly contribute to the GB population of state (n_1,n_2,n_3). GB populations are represented in terms of Ω in Figs. S3 and S4. Vertical red dashed lines correspond to Ω = 0.21 (channel (i)) and 0.16 (channel (ii)). These values lead to 100 GB trajectories. Following the definition of 1GB paths, GB trajectories are such that $p^{GB}_{n_1n_2n_3}(a_1,a_2,a_3)$ is larger than half its maximum value $1/(\pi^{3/2}\epsilon^3)$ (see Eqs. (6) and (7)). As a matter of fact, the number of available trajectories (85587 and 75277 for channels (i) and (ii), respectively) is a bit too low to obtain 100 GB trajectories for Ω = 0.1. Nevertheless, the values of Ω are sufficiently small as compared to 1 to reasonably comply with Bohr's condition of quantization.

The rest of the calculations is as previously, with the only difference that in Eq. (1) and for the H_2O+CD_3 channel, the product translational energy E_{trans} must be replaced by

$$E^{QM}_{trans} = E_{trans} + \sum_{i=1}^{3} \omega_i(a_i - \bar{a}_i). \tag{9}$$

The sum in the RHS of the above equation is the harmonic expression of the difference between the classical vibrational energy corresponding to (a_1,a_2,a_3) and the energy of vibrational quantum state $(\bar{a}_1,\bar{a}_2,\bar{a}_3)$. E^{QM}_{trans} is thus the harmonic estimation of the translational energy consistent with $(\bar{a}_1,\bar{a}_2,\bar{a}_3)$, assuming the rotational energy is correctly described by the QCT method, as is the case here ; if not, the difference between the classical and quantum rotational energies should be added to the previous difference, as detailed in the supporting information of ref. [14]. For water, the above expression works since the harmonic normal mode description is valid. For the HOD+CHD_2 channel, this description is less accurate, and the sum in Eq. (9) should better be replaced by the difference between the exact classical and quantum vibrational energies associated with $(\bar{a}_1,\bar{a}_2,\bar{a}_3)$. Substituting E^{QM}_{trans} to E_{trans} in Eq. (1) prevents from a blurring of GB-PCSDs. Such a blurring is due to the fact that, for a given rotational energy of the co-fragment (H_2O or HOD), E_{trans} is distributed broadly enough around E^{QM}_{trans} within GB. This distribution is much narrower within 1GB which, by construction, assigns negligible weights to the trajectories for which the sum in Eq. (9) significantly differs from zero.

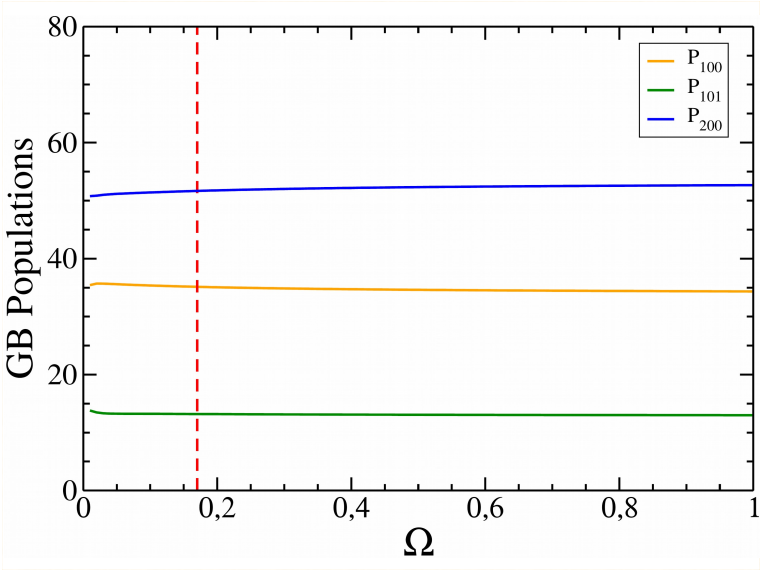

Fig. S 4: GB vibrational state populations (in percentage) of HOD in terms of Ω. The vertical red dashed line corresponds to the value of Ω (0.16) such that 100 trajectories effectively contribute to the populations.

References

[1] W. L. Hase, R. J. Duchovic, X. Komornicki, A. Hu, K. F. Lim, D.-H. Lu, G. H. Peslherbe, K. N. Swamy, S. R. Van de Linde, A. J. C. Varandas, H. Wang and R. J. Wolf, *QCPE Bull.*, 1996, **16**, 43.

[2] J. Espinosa-Garcia and J. C. Corchado, *Theor. Chem. Acc.*, 2015, **134:6**.

[3] J. Espinosa-Garcia and J. C. Corchado, *J. Phys. Chem. B*, 2016, **120**, 1446.

[4] J. C. Corchado and J. Espinosa-Garcia, *Phys. Chem. Chem. Phys.*, 2009, **11**, 10157.

[5] L. Bonnet, J. C. Corchado and J. Espinosa-Garcia, *C. R. Chim.*, 2016, **19**, 571.

[6] B. Zhang, W. Shiu and K. Liu, *J. Phys. Chem. A*, 2005, **109**, 8989.

[7] J. J. Lin, J. Zhou, W. Shiu and K. Liu, *Rev. Sci. Instrum.*, 2003, **74**, 2495.

[8] L. Bonnet, *Int. Rev. Phys. Chem.*, 2003, **32**, 171.

[9] G. Czakó and J. M. Bowman, *J. Chem. Phys.*, 2009, **131**, 244302.

[10] L. Bonnet and J. Espinosa-Garcia, *J. Chem. Phys.*, 2010, **133**, 164108.

[11] G. Czakó, *J. Phys. Chem. A*, 2012, **116**, 7467.

[12] R. Conte, B. Fu, E. Kamarchik and J. M. Bowman, *J. Chem. Phys.*, 2013, **139**, 044104.

[13] W. S. Benedict, N. Gailar and E. K. Plyler, *J. Chem. Phys.*, 1956, **24**, 1139.

[14] L. Bonnet, R. Linguerri, M. Hochlaf, O. Yazidi, P. Halvick and J. S. Francisco, *J. Phys. Chem. Lett.*, 2017, **8**, 2420.